

Fréchet Sufficient Dimension Reduction for Metric Space-Valued Data via Distance Covariance

Hsin-Hsiung Huang

Department of Statistics and Data Science, University of Central Florida, Orlando, Florida
and

Feng Yu

Department of Mathematical Science, University of Texas at El Paso, El Paso, Texas
and

Kang Li and Teng Zhang*

Department of Mathematics, University of Central Florida, Orlando, Florida

December 18, 2024

Abstract

We propose a novel Fréchet sufficient dimension reduction (SDR) method based on kernel distance covariance, tailored for metric space-valued responses such as count data, probability densities, and other complex structures. The method leverages a kernel-based transformation to map metric space-valued responses into a feature space, enabling efficient dimension reduction. By incorporating kernel distance covariance, the proposed approach offers enhanced flexibility and adaptability for datasets with diverse and non-Euclidean characteristics. The effectiveness of the method is demonstrated through synthetic simulations and several real-world applications. In all cases, the proposed method runs faster and consistently outperforms the existing Fréchet SDR approaches, demonstrating its broad applicability and robustness in addressing complex data challenges.

Keywords: bike rental, breast cancer survival, carcinoma gene expression, data visualization, global mortality rate, kernel distance covariance

*CONTACT: Teng Zhang teng.zhang@ucf.edu Department of Mathematics, University of Central Florida, Orlando, Florida 32816, U.S.A.

1 Introduction

In contemporary data analysis and visualization, the emergence of metric-space data has become increasingly prevalent in applications involving complex, non-Euclidean data objects. These objects, often termed random objects, encompass diverse forms such as count responses, probability density functions (e.g., global mortality distributions and bike rental frequencies), carcinoma gene expression profiles, and breast cancer survival statistics. The inherent complexity and non-Euclidean geometry of such data challenge the foundational assumptions of conventional statistical methods, rendering them insufficient for precise and effective analysis. Addressing these challenges necessitates the development of innovative approaches that account for the unique characteristics of metric-space data.

The concept of the Fréchet mean was introduced in 1948 (Fréchet, 1948), which extends the notion of the expectation of a random vector to random objects in a general metric space. Building on this foundational concept, Petersen and Müller proposed the Fréchet regression model (Petersen and Müller, 2019), which generalizes the Fréchet mean to conditional Fréchet means, offering a versatile framework for regression analysis with responses residing in a metric space.

Despite these advancements, the application of Fréchet regression faces the significant challenge of the curse of dimensionality, particularly when dealing with high-dimensional predictor spaces. As the number of predictors increases, the efficiency and accuracy of regression models tend to diminish, necessitating dimension reduction techniques to preserve the essential information about the predictors and their relationships with the response variable. Sufficient Dimension Reduction (SDR) techniques (Huang et al., 2024; Zhang et al., 2023), widely employed in classical regression contexts, offer a promising solution by projecting high-dimensional predictors onto a lower-dimensional subspace without losing essential information regarding the response. SDR, which is based on the conditional distribution of the response (Cook and Weisberg, 1991; Li, 1991; Xia et al., 2002; Yin and Li, 2011), achieves this by ensuring that the reduced predictors retain all the relevant regression information. Recently, Fréchet SDR methods (Ying and Yu, 2022; Zhang et al., 2023; Weng et al., 2023) have been proposed to map metric-space-valued responses to real-valued random variables using a class of functions, followed by the application of classical SDR techniques to the transformed data. These Fréchet SDR methods operate within the classical framework, where the sample size n exceeds the dimension of the predictors p . However, these methods encounter significant challenges in high-dimensional settings where p is much larger than n , particularly in relation to matrix inversion and fitting inverse regression models. First, these

methods require the inversion of a $p \times p$ covariance matrix, which becomes problematic when $p > n$ (Li and Yin, 2008). Second, interpreting the extracted components proves difficult due to the nonlinear relationships between features and responses (Tan et al., 2018; Ying and Yu, 2022).

Recent developments in SDR methods using distance covariance (dCov) (Sheng and Yin, 2013, 2016; Yang and Xu, 2024) have shown that these techniques can overcome the limitations of requiring constant covariance conditions or specific distributional assumptions for X , $X | Y$, or $Y | X$, making them broadly applicable to continuous and discrete variables across diverse distributions. Moreover, several robust SDR methods have been proposed to enhance coefficient estimation, including robust SDR using ball covariance (Zhang and Chen, 2019) and expected likelihood-based methods that minimize the Kullback-Leibler distance (Yin and Cook, 2005; Zhang and Yin, 2015).

Comparing with the functional SDR method proposed by (Yang and Xu, 2024), our approach introduces significant advancements by expanding the applicability of sufficient dimension reduction to metric-space-valued responses, providing enhanced flexibility beyond purely scalar outcomes. Specifically, our method employs kernel-based feature mapping to accommodate responses in non-Euclidean spaces, utilizing advanced kernel properties such as the Central Mean Subspace (CMS) ensembles to establish robust theoretical guarantees. Furthermore, our approach effectively addresses the curse of dimensionality through a screening method (Pan et al., 2019) that avoids the computational burden of covariance inversion, instead optimizing over Stiefel manifolds. This innovation ensures suitability for ultra-high-dimensional scenarios. While the Fréchet SDR methods (Zhang et al., 2023; Weng et al., 2023) are primarily tailored for functional data analysis, our method extends its applicability to a broader spectrum of response types, including multivariate and distributional data, thereby offering a more versatile framework.

In this paper, we present a novel sufficient dimension reduction (SDR) approach within the framework of Fréchet regression. Our method, Fd-SDR, leverages distance covariance and adopts a non-parametric strategy by mapping random objects in a metric space to real-valued random variables through a carefully selected class of functions. Compared to existing Fréchet SDR methods (Zhang et al., 2023; Weng et al., 2023), Fd-SDR demonstrates superior performance under general settings and is computationally faster. We detail our proposed method in Section 2, providing a comprehensive theoretical analysis in Section 3, including justification on kernel as well as the convergence and consistency properties. Numerical experiments validating the effectiveness of Fd-SDR on both synthetic and real datasets

are presented in Sections 4 and 5, respectively.

2 Methodology

This section presents our methodology of robust regularized Fréchet regression for sufficient dimension reduction. Section 2.1 reviews the α -dCov SDR model, and in Section 2.2, we propose our method of Fréchet SDR model via kernel distance covariance (KdCov).

2.1 Sufficient Dimension Reduction via dCov

This section reviews the classic SDR approach using the α -dCov model, in which the responses are either scalars or vectors. The α -dCov-based SDR framework generalizes the dCov method by improving robustness against data corruption caused by outliers (Huang et al., 2024). Notably, the α -dCov-based framework is reduced to the classical dCov-based SDR (Sheng and Yin, 2013, 2016) when $\alpha = 1$, and the term “dCov-based SDR” specifically refers to this case throughout this paper.

Let $\{(X_i, Y_i)\}_{i=1}^n$ be n i.i.d. samples drawn from the random variables (X, Y) . We define the data matrix $\mathbf{X} = [X_1, \dots, X_n] \in \mathbb{R}^{p \times n}$, where the columns are X_1, \dots, X_n , and let $\mathbf{Y} = [Y_1, \dots, Y_n] \in \mathbb{R}^n$ represent the vector of scalar responses. Let $\boldsymbol{\beta} \in \mathbb{R}^{p \times d}$ be the coefficient matrix and $\hat{\Sigma}_X \in \mathbb{R}^{p \times p}$ be the covariance matrix of \mathbf{X} , which is assumed to be nonsingular. The coefficient $\boldsymbol{\beta}$ of the α -dCov SDR model is obtained via maximizing the α -dCov of $\boldsymbol{\beta}^T \mathbf{X}$ and \mathbf{Y} , $\nu^2(\boldsymbol{\beta}^T \mathbf{X}, \mathbf{Y}; \alpha)$, and its empirical solution is given by solving the following optimization problem (Huang et al., 2024; Sheng and Yin, 2016):

$$\max_{\boldsymbol{\beta} \in \mathbb{R}^{p \times d}} \nu_n^2(\boldsymbol{\beta}^T \mathbf{X}, \mathbf{Y}; \alpha), \text{ s.t. } \boldsymbol{\beta}^T \hat{\Sigma}_X \boldsymbol{\beta} = \mathbf{I}_d, \quad (1)$$

where $\nu_n^2(\cdot, \cdot; \alpha)$ is the empirical α -dCov with $0 < \alpha < 2$ (Székely et al., 2007). Here, the α -dCov is defined as follows:

$$\begin{aligned} \nu^2(X, Y; \alpha) &:= \mathbb{E}[\|X - X'\|^\alpha \|Y - Y'\|^\alpha] + \mathbb{E}[\|X - X'\|^\alpha] \mathbb{E}[\|Y - Y'\|^\alpha] \\ &\quad - 2\mathbb{E}[\|X - X'\|^\alpha \|Y - Y''\|^\alpha]. \end{aligned} \quad (2)$$

and the empirical α -dCov is defined as follows. We define the distance matrices $(a_{kl}) = (\|X_k - X_l\|_2^\alpha)$, $(b_{kl}) = (\|Y_k - Y_l\|^\alpha)$ for $0 < \alpha < 2$ and $\forall k, l = 1, \dots, n$. The matrix $A \in \mathbb{R}^{n \times n}$ is defined

by

$$A_{kl} = a_{kl} - \bar{a}_{k\cdot} - \bar{a}_{\cdot l} + \bar{a}_{\cdot\cdot}, \quad \forall k, l = 1, \dots, n,$$

where the row and column means, along with the overall mean, are given by

$$\bar{a}_{k\cdot} = \frac{1}{n} \sum_{l=1}^n a_{kl}, \quad \bar{a}_{\cdot l} = \frac{1}{n} \sum_{k=1}^n a_{kl}, \quad \bar{a}_{\cdot\cdot} = \frac{1}{n^2} \sum_{k,l=1}^n a_{kl}.$$

Similarly, the matrix $B \in \mathbb{R}^{n \times n}$ is defined analogously

$$B_{kl} = b_{kl} - \bar{b}_{k\cdot} - \bar{b}_{\cdot l} + \bar{b}_{\cdot\cdot}, \quad \forall k, l = 1, \dots, n. \quad (3)$$

Using these matrices, the empirical α -dCov, $\nu_n^2(\mathbf{X}, \mathbf{Y})$, is defined by (Székely et al., 2007, Definition 4)

$$\nu_n^2(\mathbf{X}, \mathbf{Y}; \alpha) = \frac{1}{n^2} A_{kl} B_{kl}. \quad (4)$$

A computational advantage of the α -dCov approach is that the problem in (1) can be solved efficiently. Indeed, there is an alternative formulation of $\nu_n^2(\mathbf{X}, \mathbf{Y})$ (Székely et al., 2007, Appendix) as follows:

$$\nu_n^2(\mathbf{X}, \mathbf{Y}; \alpha) = S_1 + S_2 - 2S_3,$$

where

$$\begin{aligned} S_1 &= \frac{1}{n^2} \sum_{k,l=1}^n a_{kl} b_{kl}, \\ S_2 &= \frac{1}{n^2} \sum_{k,l=1}^n a_{kl} \frac{1}{n^2} \sum_{k,l=1}^n b_{kl} = \frac{1}{n^2} \sum_{k,l=1}^n a_{kl} \bar{b}_{\cdot\cdot}, \\ S_3 &= \frac{1}{n^3} \sum_{k=1}^n \sum_{l,m=1}^n a_{kl} b_{km} = \frac{1}{n^2} \sum_{k,l=1}^n a_{kl} \bar{b}_{k\cdot}. \end{aligned}$$

Notice that $\frac{1}{n^2} \sum_{k,l=1}^n a_{kl} \bar{b}_{k\cdot} = \frac{1}{n^2} \sum_{k,l=1}^n a_{kl} \bar{b}_{\cdot l}$ because for any $k, l \in [n]$, $a_{kl} \bar{b}_{k\cdot} = a_{lk} \bar{b}_{\cdot l}$. So we have

that

$$\nu_n^2(\mathbf{X}, \mathbf{Y}; \alpha) = S_1 + S_2 - 2S_3 = \frac{1}{n^2} \sum_{k,l=1}^n a_{kl}(b_{kl} + \bar{b}_{..} - \bar{b}_{k.} - \bar{b}_{.l}) = \frac{1}{n^2} a_{kl} B_{kl} \quad (5)$$

Consider the transformation $\mathbf{C} = \hat{\Sigma}_X^{\frac{1}{2}} \boldsymbol{\beta}$ and $\mathbf{Z} = \hat{\Sigma}_X^{-\frac{1}{2}} \mathbf{X}$. With the alternative formulation of the empirical dCov in (5), we can reformulate the problem in (1) as the following optimization problem:

$$\max_{\mathbf{C}} \nu_n^2(\mathbf{C}^T \mathbf{Z}, \mathbf{Y}, \alpha) := \frac{1}{n^2} \sum_{k,l=1}^n a_{kl}(\mathbf{C}; \alpha) B_{kl}, \text{ s.t. } \mathbf{C} \in \text{St}(d, p), \quad (6)$$

where $a_{kl}(\mathbf{C}; \alpha) = \|\mathbf{C}^T Z_k - \mathbf{C}^T Z_l\|_2^\alpha$ and B_{kl} is defined in (3). Here the constraint $\text{St}(d, p) = \{\mathbf{C} \in \mathbb{R}^{p \times d} \mid \mathbf{C}^T \mathbf{C} = I_d\}$ with $d \leq p$ denotes the Stiefel manifold.

2.2 Fréchet Sufficient Dimension Reduction via KdCov

The classic dCov-based SDR model is primarily designed for vector-valued responses. To accommodate metric space-valued responses, we replace the standard distance covariance with KdCov, as defined in Definition 1, and provided its empirical version in Definition 2. This concept, originally introduced by (Sejdinovic et al., 2013), differs from the standard distance covariance given in (2). Notably, the KdCov in (Sejdinovic et al., 2013) is formulated for both X and Y defining in metric spaces. In this paper, we focus on predictors X in Euclidean space, making the KdCov defined in Definition 1 a specialized case of the general framework proposed in (Sejdinovic et al., 2013).

Definition 1 (KdCov (Sejdinovic et al., 2013)). *Let $X \in \mathbb{R}^p$ be a random vector and $Y \in \mathcal{Y}$ be a metric space-valued random variable, where \mathcal{Y} is a metric space. Let $(X', Y'), (X'', Y'')$ be two i.i.d. copies drawn from the joint distribution of (X, Y) . Assume there exists a reproducing kernel Hilbert space (RKHS) \mathcal{H}_Y with an associated feature mapping $\phi : \mathcal{Y} \rightarrow \mathcal{F}$, where \mathcal{F} is a Hilbert space referred to as feature space. The kernel distance covariance (KdCov) is defined as follows:*

$$\nu_{\mathcal{H}}^2(X, Y) := \mathbb{E} [\|X - X'\| d(Y, Y')] + \mathbb{E} [\|X - X''\|] \mathbb{E} [d(Y, Y')] - 2\mathbb{E} [\|X - X'\| d(Y, Y'')], \quad (7)$$

where $d(Y, Y')$ is the distance in the feature space and is given by

$$\begin{aligned} d(Y, Y') &= \|\phi(Y) - \phi(Y')\| = \sqrt{\langle \phi(Y) - \phi(Y'), \phi(Y) - \phi(Y') \rangle} \\ &= \sqrt{\kappa(Y, Y) + \kappa(Y', Y') - 2\kappa(Y, Y')}. \end{aligned} \quad (8)$$

Here $\kappa(\cdot, \cdot) : \mathcal{Y} \times \mathcal{Y} \rightarrow \mathbb{R}$ is the kernel function, and defined by $\kappa(Y, Y') = \langle \phi(Y), \phi(Y') \rangle$.

Definition 2 (empirical KdCov). For a random sample of $(\mathbf{X}, \mathbf{Y}) = \{(X_i, Y_i)\}_{i=1}^n$ from the joint distribution of random vector $X \in \mathbb{R}^p$ and random variable $Y \in \mathcal{Y}$ where \mathcal{Y} is a metric space. Assume there exists a reproducing kernel Hilbert space (RKHS) \mathcal{H}_Y with an associated feature mapping $\phi : \mathcal{Y} \rightarrow \mathcal{F}$. Define $a_{kl} = \|X_k - X_l\|_2$, $b_{kl} = \|\phi(Y_k) - \phi(Y_l)\|_2$ for $k, l \in [n]$ and the row and column means, along with the overall mean, of a_{kl} and b_{kl} are further defined by

$$\bar{a}_{k\cdot} = \frac{1}{n} \sum_{l=1}^n a_{kl}, \quad \bar{a}_{\cdot l} = \frac{1}{n} \sum_{k=1}^n a_{kl}, \quad \bar{a}_{\cdot\cdot} = \frac{1}{n^2} \sum_{k,l=1}^n a_{kl} \quad (9)$$

$$\bar{b}_{k\cdot} = \frac{1}{n} \sum_{l=1}^n b_{kl}, \quad \bar{b}_{\cdot l} = \frac{1}{n} \sum_{k=1}^n b_{kl}, \quad \bar{b}_{\cdot\cdot} = \frac{1}{n^2} \sum_{k,l=1}^n b_{kl}. \quad (10)$$

The empirical kernel distance covariance is the nonnegative number defined by

$$\nu_{\mathcal{H},n}^2(\mathbf{X}, \mathbf{Y}) := \frac{1}{n^2} A_{kl} B_{kl},$$

where

$$A_{kl} = a_{kl} - \bar{a}_{k\cdot} - \bar{a}_{\cdot l} + \bar{a}_{\cdot\cdot}, \quad B_{kl} = b_{kl} - \bar{b}_{k\cdot} - \bar{b}_{\cdot l} + \bar{b}_{\cdot\cdot}, \quad \forall k, l = 1, \dots, n.$$

KdCov effectively characterizes the dependency structure between the predictors \mathbf{X} and the responses \mathbf{Y} in a metric space. Notably, when ϕ is the identity mapping (which is associated with the linear kernel), KdCov is reduced to the standard distance covariance defined in (2). This argument also implies that such distance can include the Wasserstein metric between distributions and Frobenius norm between matrices as special examples, since that the Wasserstein metric between distributions μ_1 and μ_2 can be considered as the ℓ_2 distance between F_1^{-1} and F_2^{-1} over $[0, 1]$, where F_i and the cumulative distribution functions of μ_i , and the Frobenius norm between matrices can be considered as the Euclidean distance between their

vectorized forms. By utilizing KdCov, the proposed SDR method is naturally extended to non-Euclidean settings, providing a more general framework for analyzing complex data structures.

To find the linear dependence between \mathbf{X} and \mathbf{Y} , we propose to maximize the KdCov of \mathbf{X} and \mathbf{Y} as follows:

$$\max_{\boldsymbol{\beta} \in \mathbb{R}^{p \times d}} \nu_{\mathcal{H}}^2(\boldsymbol{\beta}^T \mathbf{X}, \mathbf{Y}), \text{ s.t. } \boldsymbol{\beta}^T \hat{\Sigma}_X \boldsymbol{\beta} = \mathbf{I}_d, \quad (11)$$

where $\boldsymbol{\beta} \in \mathbb{R}^{p \times d}$ is the coefficient matrix and $\hat{\Sigma}_X \in \mathbb{R}^{p \times p}$ is the covariance matrix of \mathbf{X} . To solve this problem, we consider the transformation $\mathbf{C} = \hat{\Sigma}_X^{-\frac{1}{2}} \boldsymbol{\beta}$ and $\mathbf{Z} = \hat{\Sigma}_X^{-\frac{1}{2}} \mathbf{X}$, leading to the constrained maximization problem:

$$\max_{\mathbf{C} \in \mathbb{R}^{p \times d}} \nu_{\mathcal{H},n}^2(\mathbf{C}^T \mathbf{Z}, \mathbf{Y}) := F(\mathbf{C}), \text{ s.t. } \mathbf{C} \in \text{St}(d, p), \quad (12)$$

where $\text{St}(d, p) = \{\mathbf{C} \in \mathbb{R}^{p \times d} \mid \mathbf{C}^T \mathbf{C} = \mathbf{I}_d\}$ with $d \leq p$ is the Stiefel manifold and $\nu_{\mathcal{H},n}^2(\cdot, \cdot)$ represents the empirical KdCov provided in Definition 2. Similar to the empirical dCov, the empirical KdCov also admits an alternative formulation. Following the formulas in Definition 2, the objective $F(\mathbf{C})$ in (12) is given by

$$F(\mathbf{C}) := \frac{1}{n^2} \sum_{k,l=1}^n A_{kl}(\mathbf{C}) B_{kl}, \quad (13)$$

where $A_{kl}(\mathbf{C})$ and B_{kl} are provided in (9) and (10) respectively with $a_{kl}(\mathbf{C}) = \|\mathbf{C}^T Z_k - \mathbf{C}^T Z_l\|_2 = \|\boldsymbol{\beta}^T X_k - \boldsymbol{\beta}^T X_l\|_2$ and $b_{kl} = \|\phi(Y_k) - \phi(Y_l)\|_2$. If we apply the kernel function κ on $\{Y_i\}_{i=1}^n$ to obtain the kernel matrix $\mathbf{K} \in \mathbb{R}^{n \times n}$ and find its square root $\mathbf{M} = \mathbf{K}^{1/2} \in \mathbb{R}^{n \times n}$, we have that $F(\mathbf{C}) = \nu_{\mathcal{H},n}^2(\mathbf{C}^T \mathbf{Z}, \mathbf{Y}) = \nu_n^2(\mathbf{C}^T \mathbf{Z}, \mathbf{M})$, which follows from $\|\mathbf{M}(:, k) - \mathbf{M}(:, l)\|_2^2 = \mathbf{M}(:, k)^T \mathbf{M}(:, k) + \mathbf{M}(:, l)^T \mathbf{M}(:, l) - 2\mathbf{M}(:, k)^T \mathbf{M}(:, l) = \mathbf{K}(k, k) + \mathbf{K}(l, l) - 2\mathbf{K}(k, l) = \|\phi(Y_k) - \phi(Y_l)\|_2^2$. Combining with (5), we are able to reformulate the problem (12) as follows:

$$\max_{\mathbf{C} \in \mathbb{R}^{p \times d}} F(\mathbf{C}) = \frac{1}{n^2} \sum_{k,l=1}^n a_{kl}(\mathbf{C}) \tilde{B}_{kl}, \text{ s.t. } \mathbf{C} \in \text{St}(d, p), \quad (14)$$

where $a_{kl}(\mathbf{C}) = \|\mathbf{C}^T Z_k - \mathbf{C}^T Z_l\|_2$ and \tilde{B}_{kl} is given in (3) with $\tilde{b}_{kl} = \|\mathbf{M}(:, k) - \mathbf{M}(:, l)\|_2 = \|\phi(Y_k) - \phi(Y_l)\|_2$. It is worth noting that the matrix \tilde{B} , constructed using $\tilde{b}_{kl} = \|\mathbf{M}(:, k) - \mathbf{M}(:, l)\|_2$, is identical

to the matrix B constructed using $b_{kl} = \|\phi(Y_k) - \phi(Y_l)\|_2$. The distinction in notation is introduced to emphasize their respective contexts: \tilde{B} is employed in the empirical distance covariance, $\nu_n^2(\mathbf{C}^T \mathbf{Z}, \mathbf{M})$, whereas B is used in the empirical kernel distance covariance, $\nu_{\mathcal{H},n}^2(\mathbf{C}^T \mathbf{Z}, \mathbf{Y})$. This differentiation helps clarify the role of each matrix in their respective formulations.

Kernel Selection

We provide two kernel functions in Algorithm 1: the Gaussian kernel and the Laplacian kernel, defined respectively as

$$\kappa_G(Y, Y') = \exp(-\gamma_G \cdot d(Y, Y')^2), \quad \kappa_L(Y, Y') = \exp(-\gamma_L \cdot d(Y, Y')),$$

where $d(Y, Y')$ represents the distance between Y and Y' in the metric space \mathcal{Y} . The choice of distance $d(Y, Y')$ is data-dependent, with the Wasserstein distance used for distributional data and the Frobenius norm for matrix data. These selections align with the definition of $d(Y, Y')$ in metric spaces, ensuring compatibility with various data modalities.

Bandwidth Selection

Following the recommendations in (Zhang et al., 2023), the kernel bandwidths γ_G and γ_L are computed as

$$\gamma_G = \frac{\rho_Y}{2\sigma_G^2}, \quad \gamma_L = \frac{\rho_Y}{2\sigma_L},$$

where ρ_Y is a scaling parameter (commonly set to 10), and σ_G^2 and σ_L are defined as

$$\sigma_G^2 = \binom{n}{2}^{-1} \sum_{i < j} d(Y_i, Y_j)^2, \quad \sigma_L = \binom{n}{2}^{-1} \sum_{i < j} d(Y_i, Y_j).$$

These formulas ensure that the bandwidths are tailored to the data's distribution and scale, enhancing the performance of the kernel functions in capturing dependencies. By incorporating the flexibility of different distances and kernels, this framework is adaptable to a wide range of applications and data structures.

The constrained maximization problem in (14) can be solved via various routines such as the conjugate gradient and steepest descent. For completeness, we present the formula for the steepest descent

algorithm. Specifically, each (sub)gradient descent step is followed by a projection onto the Stiefel manifold: $\mathbf{C}^{(\text{iter}+1)} = P_S\left(\mathbf{C}^{(\text{iter})} + \alpha^{(\text{iter})}\partial_{\mathbf{C}}F(\mathbf{C}^{(\text{iter})})\right)$, where $P_S(\cdot)$ denotes the projection on the Stiefel manifold and $\alpha^{(\text{iter})}$ is the optimal step-size obtained from the backtracking line search (Absil et al., 2008). According to (Absil and Malick, 2012, Proposition 3.4), the projection of \mathbf{C} onto $\text{St}(d, p)$ exists uniquely and can be expressed as $P_S(\mathbf{C}) = \mathbf{U}\mathbf{V}^T$ if the SVD of $\mathbf{C} \in \mathbb{R}^{p \times d}$ is given by $\mathbf{C} = \mathbf{U}\mathbf{\Sigma}\mathbf{V}^T$. Additionally, the explicit formula for the subgradient $\partial_{\mathbf{C}}F(\mathbf{C})$, where $F(\mathbf{C})$ is defined in (14), is derived as follows:

$$\partial_{\mathbf{C}}F(\mathbf{C}) = \frac{1}{n^2} \sum_{k,l=1}^n (\partial[\|\mathbf{C}^T Z_k - \mathbf{C}^T Z_l\|_2]) \tilde{B}_{kl} = \frac{1}{n^2} \sum_{k \neq l} \frac{\mathbf{C}^T(Z_k - Z_l)(Z_k - Z_l)^T}{\|\mathbf{C}^T(Z_k - Z_l)\|_2} \tilde{B}_{kl}, \quad (15)$$

where we assume $Z_k \neq Z_l$ for all $k, l \in [n]$, considering only the corresponding case for the subgradient $\partial[\|\mathbf{C}^T Z_k - \mathbf{C}^T Z_l\|_2]$. We summarize the algorithm for Fréchet SDR via KdCov (Fd-SDR) in Algorithm 1.

Algorithm 1 Fd-SDR

- 1: **Input:** The samples $\{(X_i, Y_i)\}_{i=1}^n \subset \mathbb{R}^p \times \mathcal{Y}$, kernel function $\kappa : \mathcal{Y} \times \mathcal{Y} \rightarrow \mathbb{R}$, target dimension: $d(< p)$, maximum number of iterations: K , stopping threshold: ε .
 - 2: **Preparation:** Compute the sample covariance $\hat{\Sigma}_X$ and $\mathbf{Z} = \hat{\Sigma}_X^{-\frac{1}{2}}\mathbf{X}$; compute the kernel matrix $\mathbf{K} \in \mathbb{R}^{n \times n}$, where $\mathbf{K}_{ij} = \kappa(Y_i, Y_j), \forall i, j \in [n]$ and $\mathbf{M} = \mathbf{K}^{1/2} \in \mathbb{R}^{n \times n}$.
 - 3: **Initialization:** $\mathbf{C}^{(0)}$.
 - 4: **for** iter = 0, 1, ..., K **do**
 - 5: Compute $\mathbf{C}^{(\text{iter}+1)} = P_S\left(\mathbf{C}^{(\text{iter})} + \alpha^{(\text{iter})}\partial_{\mathbf{C}}F(\mathbf{C}^{(\text{iter})})\right)$, where $\partial_{\mathbf{C}}F(\mathbf{C})$ is defined by (15), \tilde{B}_{kl} is given in (3) with $\tilde{B}_{kl} = \|\mathbf{M}(:, k) - \mathbf{M}(:, l)\|$ and $\alpha^{(\text{iter})}$ is obtained by backtracking line search method.
 - 6: Stop if $\|F(\mathbf{C}^{(\text{iter}+1)}) - F(\mathbf{C}^{(\text{iter})})\|_F \leq \varepsilon$.
 - 7: **end for**
 - 8: **Output:** Estimated coefficient matrix $\hat{\beta} = \hat{\Sigma}_X^{-\frac{1}{2}}\mathbf{C}^{(\text{iter})}$.
-

2.3 Comparison with other Fréchet SDR methods

In this section, we primarily compare our proposed method, Fd-SDR, with two other Fréchet sufficient dimension reduction (SDR) methods, Fréchet OPG (FOPG) (Zhang et al., 2023) and Graphical Weighted Inverse Regression Ensemble (GWIRE) (Weng et al., 2023), in terms of the computational complexity and implementation. FOPG demonstrates state-of-the-art performance across general settings for Fréchet

SDR methods, while GWIRE performs effectively in sparse settings, where an additional assumption is made that the coefficient matrix β is sparse.

2.3.1 Computational Comparison

Our proposed method, detailed in Algorithm 1, demonstrates computational superiority over FOPG and GWIRE. The computational complexity of the preparation step is $O(n^3 + n^2p)$, primarily due to the computation of the kernel matrix and its square root. Step 5 in Algorithm 1 involve the optimization over the Stiefel manifold and gradient updates, with a complexity of $O(n^2pd + pd^2)$. In comparison, FOPG (Zhang et al., 2023, Algorithm 2) requires solving n^2 regression problems in Step 2, which has a computational cost of $O(n^3p)$ and the calculation of $\Lambda^{(t)}$ in Step 3 requires $O(n^2p^2)$, and performing eigenvalue decomposition requires $O(p^2d)$. Consequently, its per-iteration cost is at least $O(n^2p(n + p) + p^2d)$, which is larger than the per-iteration cost of Algorithm 1. GWIRE requires a per-iteration cost $O(p^3)$, with an additional cost of $O(np^2)$ for computing the sample covariance. However, its performance highly depends on the a regularization parameter, while our method is parameter-free. The implementation of GWIRE requires choosing a regularization parameter by 5-fold cross-validation over 30 candidates and is therefore usually much slower than Algorithm 1 in practice.

2.3.2 Implementation Comparison

Our method shares some similarity with the Fréchet sufficient dimension reduction (SDR) approach proposed in (Zhang et al., 2023). However, since we utilize the distance covariance matrix and base our algorithm on (Huang et al., 2024), the two methods exhibit key differences. In (Zhang et al., 2023), Fréchet SDR is applied using $\kappa(Y, \cdot)$ as the response, which distinguishes it from classical SDR techniques, while our method utilizes the feature map $\phi(Y)$ as the response.

Traditional SDR assumes Y is a real-valued response, so these methods can not be directly applied to Fréchet SDR, where Y is a metric space-valued response. To handle metric space-valued response, the method in (Zhang et al., 2023) proposes to find the a class of real-valued functions \mathcal{F} and then use

$$\bigcup \{S_{E[f(Y)|X]} : f \in \mathcal{F}\}$$

as the estimator of the central subspace. Here $E(Y|X)$ is called mean dimension reduction subspace,

a weaker form of SDR introduced in (Cook and Li, 2002) and defined as the subspace S such that $E(Y|X) = E(Y|P_S X)$. Note that $S_{E[f(Y)|X]}$ can be estimated using traditional methods as $f(Y)$ is real-valued, so we can turn an SDR method that targets real-valued responses into one that targets metric space-valued responses, and find the Fréchet central subspace.

The method in (Zhang et al., 2023) proposes to use $\mathcal{F} = \{\kappa(\cdot, y) : y \in \Omega_Y\}$, where κ is a RHKS, and the method implemented as follows. Let F_{XY} is the empirical distribution of observations and F_Y is the empirical distribution of Y , then the proposed estimator of the Fréchet central subspace $S_{Y|X}$ is

$$M(F_{XY}) = \int_{\Omega_Y} M_0(F_{XY}, \kappa(\cdot, y)) dF_Y(y), \quad (16)$$

where $M_0(F_{XY}, \kappa(\cdot, y))$ is the estimator of classical SDR central subspace with responses

$$\kappa(Y_1, y), \dots, \kappa(Y_n, y).$$

3 Theoretical Guarantees

In this section, we present three theoretical results for the proposed Fd-SDR method outlined in Algorithm 1: 1) The justification for performing Fréchet SDR using feature map-based responses $\{\phi(Y_i)\}_{i=1}^n$ is established in Theorem 1; 2) The statistical consistency of Fd-SDR under the model specified in (20) is provided in Theorem 2; 3) The algorithmic convergence result for Fd-SDR is presented in Theorem 3.

Our theoretical guarantee is based on the concept of CMS-Ensemble, introduced by Zhang et al. in (Zhang et al., 2023) as follows.

Definition 3 (Definition of CMS-Ensemble). *The Central Mean Space ensemble (CMS-ensemble) is defined as a family \mathcal{F} that is rich enough so that*

$$S_{Y|X} = \bigcup \{S_{E[f(Y)|X]} : f \in \mathcal{F}\}. \quad (17)$$

Recall that $S_{E[f(Y)|X]}$ is the mean dimension reduction subspace defined in Section 2.3.2.

This definition implies that the ensemble \mathcal{F} is a collection of functions rich enough such that the union of the spaces $S_{E[f(Y)|X]}$ captures the full central subspace $S_{Y|X}$. In addition, (Zhang et al., 2023) proves that for a large range of kernels and Ω_Y , the family $\mathcal{F} = \{\kappa(\cdot, y) : y \in \Omega_Y\}$ constitutes a CMS-ensemble.

In particular, they prove that this holds as long as (1) κ is a bounded, compact-convergence (cc)-universal kernel (cc-universal implies that the RKHS associated with κ is sufficiently rich to approximate any compactly supported continuous function in ℓ_∞ norm, and we refer readers to (Micchelli et al., 2006; Sriperumbudur et al., 2011) for formal definition), and (2) P_Y is a regular probability measure. We refer the interested reader to (Zhang et al., 2023) for more technical details.

Theorem 1 shows that when the kernel is a CMS-ensemble, the central subspace defined by the original responses \mathbf{Y} coincides with that defined by their feature map representations $\phi(\mathbf{Y})$. It guarantees the performance of the proposed Fd-SDR Algorithm, as its objective function is derived from dCov-based SDR by replacing response Y with its feature map $\phi(Y)$, see (13). Following (Zhang et al., 2023), a wide range of kernels fall into the CMS-ensemble category, including Gaussian and Laplacian kernels in various spaces such as the Euclidean space, Wasserstein space, the space of symmetric positive definite matrices, and the sphere. Notably, this result pertains to the central subspace and is independent of the specific algorithm used, ensuring broad applicability.

Theorem 1 (Theoretical guarantee for Fd-SDR Algorithm and feature map-based SDR). *Let $\mathcal{S}_{Y|X}$ represent the central subspace of random variables (X, Y) , and κ is a RKHS. If the family of functions $\{\kappa(\cdot, \mathbf{Y}) : \mathbf{Y} \in \mathcal{Y}\}$ is a CMS-ensemble, then $\mathcal{S}_{\phi(Y)|X} = \mathcal{S}_{Y|X}$, where ϕ is the feature map induced by the RKHS κ .*

Proof of Theorem 1. Let $S = \mathcal{S}_{Y|X}$, then by definition, $Y \perp\!\!\!\perp X|P_S X$, and as a result, $\phi(Y) \perp\!\!\!\perp X|P_S X$ and

$$\mathcal{S}_{\phi(Y)|X} \subseteq \mathcal{S}_{Y|X}. \quad (18)$$

As $\kappa(Y, Y_0) = \langle \phi(Y), \phi(Y_0) \rangle$, we have that for all $Y_0 \in \mathcal{Y}$,

$$\mathcal{S}_{\kappa(Y, Y_0)|X} \subseteq \mathcal{S}_{\phi(Y)|X}$$

and

$$\mathcal{S}_{Y|X} = \text{span}(\mathcal{S}_{\kappa(Y, Y_0)|X} : Y_0 \in \mathcal{Y}) \subseteq \mathcal{S}_{\phi(Y)|X}, \quad (19)$$

where the first equality follows from the assumption that the family of functions $\{\kappa(\cdot, \mathbf{Y}) : \mathbf{Y} \in \mathcal{Y}\}$ is a CMS-ensemble. Combining (18) and (19), the theorem is proved. \square

Our second result establishes the consistency of Algorithm 1. Following (Huang et al., 2024), we

consider a model with a general noise term

$$\mathbf{Y} = g(\boldsymbol{\beta}_0^T \mathbf{X}, \epsilon) = g(\mathbf{C}_0^T \mathbf{Z}, \epsilon), \quad (20)$$

where $\boldsymbol{\beta}_0$ is a $p \times d$ orthogonal matrix, $g(\cdot)$ is an unknown link function, $\mathbf{C}_0 = \hat{\Sigma}_X^{\frac{1}{2}} \boldsymbol{\beta}_0$, and $\mathbf{Z} = \hat{\Sigma}_X^{-\frac{1}{2}} \mathbf{X}$, and ϵ is independent of \mathbf{Z} . This model includes the model from (Xia et al., 2002) that $\mathbf{Y} = g(\boldsymbol{\beta}_0^T \mathbf{X}) + \epsilon$ is a special example.

The theorem on the asymptotic properties of our estimator \mathbf{C} up to some rotation matrix \mathbf{Q} in (Huang et al., 2024, Proposition 3.1) also applies to our setting, which implies the asymptotic property of the estimated central subspace.

Theorem 2 (Consistency guarantee for Fd-SDR Algorithm). *Under model (20), and let $\mathbf{C} \in \mathbb{R}^{d \times p}$ be a basis of the central subspace $S_{Y|X}$ with $\mathbf{C}^T \Sigma_{\mathbf{X}} \mathbf{C} = \mathbf{I}_d$. Suppose $P_{\mathbf{C}(\Sigma_{\mathbf{X}})}^T \mathbf{X} \perp\!\!\!\perp Q_{\mathbf{C}(\Sigma_{\mathbf{X}})}^T \mathbf{X}$ and the support of $\mathbf{X} \in \mathbb{R}^{d \times p}$, say S , is a compact set. In addition, assume that there exists $\mathbf{C}' \in \mathbb{R}^{(p-d) \times p}$ such that $[\mathbf{C}, \mathbf{C}']^T \Sigma_{\mathbf{X}} [\mathbf{C}, \mathbf{C}'] = \mathbf{I}_p$ and $\mathbf{C}^T \mathbf{X}$ is independent of $\mathbf{C}'^T \mathbf{X}$. Let $\hat{\mathbf{C}}_n = \arg \min_{\mathbf{C}^T \Sigma_{\mathbf{X}} \mathbf{C} = \mathbf{I}_d} \nu_n^2(\mathbf{C}^T \mathbf{X}, \mathbf{Y})$, then there exists a rotation matrix \mathbf{Q} : $\mathbf{Q}^T \mathbf{Q} = \mathbf{I}_d$ such that $\hat{\mathbf{C}}_n \xrightarrow{P} \mathbf{C} \mathbf{Q}$ (convergence in probability) as $n \rightarrow \infty$, with a rate of $1/\sqrt{n}$: $\min_{\mathbf{Q}} \|\hat{\mathbf{C}}_n - \mathbf{C} \mathbf{Q}\|_F = O_p(1/\sqrt{n})$.*

Proof of Theorem 2. First, we note that our method is rSDR (Huang et al., 2024) with responses being $\phi(Y)$. Since our response $\phi(Y) = \phi(g(\boldsymbol{\beta}_0^T \mathbf{X}, \epsilon))$ is also a function of $\boldsymbol{\beta}_0^T \mathbf{X}$ and ϵ , the proof of convergence follows from (Huang et al., 2024, Proposition 3.1).

Next, we prove the convergence rate $1/\sqrt{n}$. The minimization of the empirical risk function implies that the difference $\hat{\mathbf{C}}_n - \mathbf{C} \mathbf{Q}$ becomes small as $n \rightarrow \infty$. More precisely, using Taylor expansion around the true parameter \mathbf{C} , we have

$$\nu_n^2(\hat{\mathbf{C}}_n^T \mathbf{X}, \mathbf{Y}) - \nu_n^2(\mathbf{C}^T \mathbf{X}, \mathbf{Y}) = O_p(1/n).$$

This indicates that the difference $\hat{\mathbf{C}}_n - \mathbf{C} \mathbf{Q}$ is of order $O_p(1/\sqrt{n})$. Finally, to conclude that $\|\hat{\mathbf{C}}_n - \mathbf{C} \mathbf{Q}\|_F = O_p(1/\sqrt{n})$, we apply standard results from matrix perturbation theory (Stewart, 1990). Since $\hat{\mathbf{C}}_n$ is constrained by $\hat{\mathbf{C}}_n^T \Sigma_{\mathbf{X}} \hat{\mathbf{C}}_n = \mathbf{I}_d$, the difference between $\hat{\mathbf{C}}_n$ and $\mathbf{C} \mathbf{Q}$ is bounded in the Frobenius norm by the rate of convergence of the empirical risk function, which yields the desired result. Thus, we have established that

$$\min_{\mathbf{Q}} \|\hat{\mathbf{C}}_n - \mathbf{C} \mathbf{Q}\|_F = O_p(1/\sqrt{n}).$$

□

Similar to (Huang et al., 2024, Proposition 3.1), Theorem 2 requires an additional assumption related to the decomposition of X into two independent components. Further discussion on this condition can be found in (Sheng and Yin, 2013, Section 3.2). For instance, this assumption holds when X follows a normal distribution (Zhang and Yin, 2015) and is asymptotically satisfied when p is large, as shown in (Hall and Li, 1993).

Our final result establishes the algorithmic convergence of Algorithm 1. Since Fd-SDR is based on the algorithm proposed in (Huang et al., 2024), its theoretical guarantee in (Huang et al., 2024, Theorem 3.2) can be easily generalized to our setting, which states that any accumulation point is a stationary point of the objective function.

Theorem 3 (Convergence of Fd-SDR Algorithm). *(a) Any accumulation point of the sequence $\{\hat{\mathbf{C}}^{(t)}\}_{t \geq 0}$ generated by the proposed algorithm converges is a stationary point of $F_\eta(\mathbf{C})$ over the Stiefel manifold, the set of all orthogonal matrices of size $\mathbb{R}^{p \times d}$.*

(b) If in addition, the global maximizer $\hat{\mathbf{C}}$ is the unique stationary point in its neighborhood \mathcal{N} , and $F_\eta(\mathbf{C}) - F_\eta(\hat{\mathbf{C}}) \leq -c\|\mathbf{C} - \hat{\mathbf{C}}\|_F^2$ for any \mathbf{C} in \mathcal{N} and some $c > 0$. Then when the initialization $\hat{\mathbf{C}}^{(0)}$ is sufficiently close to $\hat{\mathbf{C}}$, the sequence $\{\hat{\mathbf{C}}^{(t)}\}_{t \geq 0}$ converges to $\hat{\mathbf{C}}$.

4 Simulation Studies

In this section, we compare the performance of the proposed Fd-SDR method with FOPG (Zhang et al., 2023) and GWIRE (Weng et al., 2023) in terms of accuracy across the different synthetic settings described in Sections 4.1-4.3. Additionally, we provide a comparison of the computational efficiency in Section 4.4.

4.1 Scenario I: SDR for distributions

We set $\beta_1 = (1, 1, 0, \dots, 0)^T$, $\beta_2 = (0, \dots, 0, 1, 1)^T$, $\beta_3 = (1, 2, 0, \dots, 0, 2)^T$, and $\beta_4 = (0, 0, 1, 2, 2, 0, \dots, 0)^T$ in \mathbb{R}^p . Additionally, we let $Y \sim \mathcal{N}(\mu_Y, \alpha\sigma_Y^2)$, where μ_Y and σ_Y are random variables depending on X . Denote the Fréchet central subspace by \mathcal{S} and its estimation with $\hat{\mathcal{S}}$. The following four models are considered:

- (1) $\mu_Y \sim \mathcal{N}(\exp(\beta_1^T X), 0.1)$, $\sigma_Y = 0.5$, $\alpha = 1$ and $\mathcal{S} = [\beta_1]$.
- (2) $\mu_Y \sim \mathcal{N}(\exp(\beta_1^T X), 0.1)$, $\sigma_Y = \exp(\beta_2^T X)$ with truncated range $(10^{-1}, 10)$, $\alpha = 1$ and $\mathcal{S} = [\beta_1, \beta_2]$.
- (3) $\mu_Y \sim \mathcal{N}(3(\beta_3^T X), 0.5^2)$, $\sigma_Y = \text{Gamma}((2 + 2\beta_4^T X)^2/\nu, \nu/(2 + 2\beta_4^T X))$ with truncated range $(10^{-1}, 10)$ and $\nu = 0.5$, $\alpha = 0.2/0.4$ and $\mathcal{S} = [\beta_3, \beta_4]$.
- (4) $\mu_Y \sim \mathcal{N}(3 \sin(\beta_3^T X), 0.5^2)$, $\sigma_Y = \text{Gamma}((2 + 2\beta_4^T X)^2/\nu, \nu/(2 + 2\beta_4^T X))$ with truncated range $(10^{-1}, 10)$ and $\nu = 0.5$, $\alpha = 0.2/0.4$ and $\mathcal{S} = [\beta_3, \beta_4]$.

We consider three different approaches for generating the predictor X :

- (a) $X \sim \mathcal{N}(0, \mathbf{I}_p)$.
- (b) Generate U_1, U_2, \dots, U_p from AR(1) model with mean 0 and covariance $\Sigma = (0.5^{|i-j|})_{i,j}$, then set $X = (\sin(U_1), |U_2|, U_3, \dots, U_p)$.
- (c) Generate U_1, U_2, \dots, U_p from AR(1) model with mean 0 and covariance $\Sigma = (0.5^{|i-j|})_{i,j}$, then set $X = [\Phi(U_1), \dots, \Phi(U_p)]$, where $\Phi(\cdot)$ is the c.d.f. of the standard normal distribution.

We generate the set of samples $\{(X_i, Y_i)\}_{i=1}^n$ following models above. For Models (1) and (2), we use approaches (a) and (b) to generate X . For Models (3) and (4), approach (c) is used to generate X . The estimated Fréchet central subspace $\hat{\mathcal{S}}$ is obtained using Fd-SDR, FOPG, and GWIRE with the Gaussian kernel $\kappa_G(Y, Y') = \exp(-\gamma_G \cdot d(Y, Y')^2)$. Details on the choice of bandwidth and related specifications can be found in Section 2.2. The estimation error is defined by the Frobenius norm of the difference between the projectors on \mathcal{S} and $\hat{\mathcal{S}}$: $e(\mathcal{S}, \hat{\mathcal{S}}) = \|P_{\mathcal{S}} - P_{\hat{\mathcal{S}}}\|_F = \|B(B^T B)^{-1} B^T - \hat{B}(\hat{B}^T \hat{B})^{-1} \hat{B}^T\|_F$. We repeat the simulation 100 times for two cases, $(n, p) = (200, 10)$ and $(n, p) = (400, 20)$, and report the mean errors as well as the standard deviations in Table 1. The box plots comparing the errors of the three estimators are shown in Figure 1.

The results in Table 1 demonstrate that Fd-SDR achieves smaller estimation errors than FOPG and GWIRE in most models, with a few exceptions where Fd-SDR remains competitive. Especially in Model (3-c) and (4-c), Fd-SDR can estimate the accurate subspace while other two estimators fail. In these two models, the errors for both FOPG and GWIRE increase significantly as the value of α decreases while Fd-SDR still leads to a good estimation. We present the box plots in Figure 1 for these two models

(n, p)	Model	Fd-SDR	FOPG	GWIRE
(200,10)	(1-a)	0.09(0.03)	0.16(0.08)	0.07(0.05)
	(1-b)	0.09(0.03)	0.11(0.04)	0.20(0.06)
	(2-a)	0.18(0.03)	0.25(0.12)	0.23(0.07)
	(2-b)	0.25(0.07)	0.27(0.06)	0.71(0.20)
	(3-c), $\alpha = 0.2$	0.45(0.17)	1.39(0.03)	0.89(0.17)
	(3-c), $\alpha = 0.4$	0.30(0.06)	0.70(0.36)	0.67(0.12)
	(4-c), $\alpha = 0.2$	0.36(0.07)	1.29(0.15)	0.72(0.14)
	(4-c), $\alpha = 0.4$	0.34(0.07)	0.29(0.07)	0.62(0.08)
(400,20)	(1-a)	0.09(0.02)	0.22(0.05)	0.05(0.04)
	(1-b)	0.09(0.02)	0.18(0.03)	0.20(0.05)
	(2-a)	0.22(0.03)	0.29(0.09)	0.13(0.06)
	(2-b)	0.26(0.05)	0.33(0.05)	0.64(0.15)
	(3-c), $\alpha = 0.2$	0.40(0.08)	1.40(0.03)	0.86(0.17)
	(3-c), $\alpha = 0.4$	0.30(0.04)	0.92(0.35)	0.64(0.09)
	(4-c), $\alpha = 0.2$	0.35(0.05)	1.36(0.10)	0.69(0.10)
	(4-c), $\alpha = 0.4$	0.34(0.05)	0.29(0.05)	0.59(0.05)

Table 1: Errors of Fd-SDR, FOPG and GWIRE in mean and standard deviation (in parentheses) for Scenario I.

with $n = 400$. The plot indicates that Fd-SDR has smaller mean and variance over the 100 repeated simulations and has few outliers than FOPG and GWIRE. Moreover, we notice that GWIRE shows the smallest estimation errors in Model (1-a) for both of $(n, p) = (200, 10)$ and $(n, p) = (400, 20)$. However, GWIRE fails and has large errors especially in Model (3-c) and (4-c), which is mainly because GWIRE assumes the sparsity of the subspace, an assumption that these two models do not satisfy. The results highlight that Fd-SDR is able to estimate the Fréchet central subspace and has better performance compared to the existing FSDR methods across various models, making it a reliable method in general.

4.2 Scenario II: SDR for matrices

In this synthetic dataset, we use similar settings to those in Scenario I, but with a modification in how the response Y is generated. Specifically, the vectors β_1 and β_2 , as well as the approaches (a) and (b) for generating X from Scenario I, are retained. We set $\log(Y) \sim \mathcal{N}_{q \times q}(\log(D(X)), 0.5^2 \mathbf{I}_q)$, where two

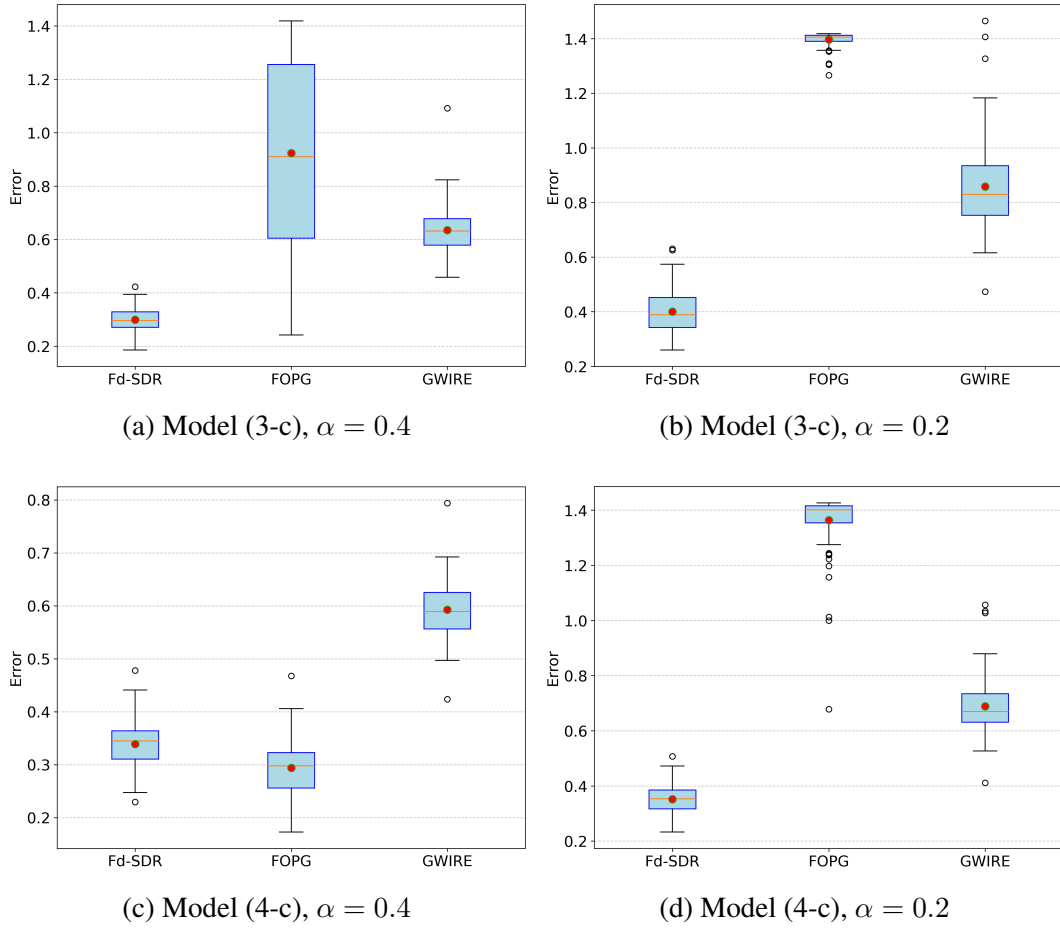


Figure 1: Box plots of Fd-SDR, FOPG and GWIRE in Models (3-c) and (4-c) with $n = 400$ from Scenario I.

models of $D(X)$ are defined:

$$(1) D(X) = \begin{bmatrix} 1 & \rho(X) \\ \rho(X) & 1 \end{bmatrix}, \text{ where } \rho(X) = 0.8 \cos(\beta_1^T X), \text{ and } \mathcal{S} = [\beta_1].$$

$$(2) D(x) = \begin{bmatrix} 1 & \rho_1(X) & \rho_2(X) \\ \rho_1(X) & 1 & \rho_1(X) \\ \rho_2(X) & \rho_1(X) & 1 \end{bmatrix}, \text{ where } \rho_1(X) = 0.8 \cos(\beta_1^T X), \rho_2(X) = 0.8 \sin(\beta_2^T X), \text{ and } \mathcal{S} = [\beta_1, \beta_2].$$

Here $\mathcal{N}_{q \times q}(M, \Sigma)$ with symmetric mean M and covariance Σ refers to the symmetric matrix variate normal distribution (Schwartzman, 2006). The p.d.f. of $Z \sim \mathcal{N}_{q \times q}(M, \Sigma)$ is given by

$$f(z; M, \Sigma) = \frac{1}{(2\pi)^{p/2} |\Sigma|^{(q+1)/2}} \exp\left(-\frac{1}{2} \text{tr}((z - M)\Sigma^{-1})^2\right),$$

where $p = q(q + 1)/2$.

Similar to Scenario I, we estimate Fréchet central subspace using Fd-SDR, FOPG, and GWIRE with the Gaussian kernel $\kappa_G(Y, Y') = \exp(-\gamma_G \cdot d(Y, Y')^2)$. The simulation is repeated 100 times, and the means and standard deviations of the estimation errors for the three estimators are summarized in Table 2. The results of this table show that Fd-SDR outperforms the other two methods and the errors in Model (2) are noticeable smaller than FOPG and GWIRE with the only exception in Model (1-b). Even in this model, Fd-SDR only has slightly large errors. We remark that GWIRE is not applicable (NA) for Model (1-a) as it fails to select the regularization parameter.

(n, p)	Model	Fd-SDR	FOPG	GWIRE
(200,10)	(1-a)	0.24(0.29)	0.30(0.33)	NA
	(1-b)	0.22(0.08)	0.24(0.10)	0.20(0.06)
	(2-a)	0.30(0.07)	0.37(0.23)	1.35(0.14)
	(2-b)	0.43(0.12)	0.67(0.37)	0.72(0.19)
(400,20)	(1-a)	0.36(0.44)	0.52(0.49)	NA
	(1-b)	0.24(0.07)	0.24(0.10)	0.20(0.07)
	(2-a)	0.45(0.35)	0.66(0.47)	1.41(0.04)
	(2-b)	0.44(0.07)	0.74(0.34)	0.69(0.14)

Table 2: Errors of Fd-SDR, FOPG and GWIRE in mean and standard deviation (in parentheses) for Scenario II.

4.3 Scenario III: SDR for spherical data

In this simulation, we use similar settings to those in Scenario I, but with modifications to the subspace vectors and the way the response Y is generated. The approaches (a) and (c) for generating X from Scenario I are applied. Let $\beta_1 = \frac{1}{\sqrt{3}}(x_1, x_2, x_3, 0, \dots, 0)^T$, $\beta_2 = \frac{1}{\sqrt{3}}(0, \dots, 0, x_{p-2}, x_{p-1}, x_p)^T$ and $\beta_3 = (0, 1, 0, \dots, 0)^T$ with $x_i \stackrel{i.i.d.}{\sim} \mathcal{N}(0, 1)$. We generate the spherical data Y from the following three

models:

- (1) Y is generated by $Y = \cos(\|\varepsilon(X)\|)m(X) + \sin(\|\varepsilon(X)\|)\frac{\varepsilon(X)}{\|\varepsilon(X)\|}$ where $m(X), \varepsilon(X)$ are given by

$$\begin{aligned} m(X) &= (\cos(\pi\beta_1^T X), \sin(\pi\beta_1^T X)) \\ \varepsilon(X) &= (-\delta \sin(\pi\beta_1^T X), \delta \cos(\pi\beta_1^T X)) \end{aligned}$$

with $\delta \sim N(0, 0.2^2)$. The underlying subspace is $\mathcal{S} = [\beta_1]$.

- (2) Y is generated by $Y = \cos(\|\varepsilon\|)m(X) + \sin(\|\varepsilon\|)\frac{\varepsilon}{\|\varepsilon\|}$ where $m(X), \varepsilon$ are given by

$$\begin{aligned} m(X) &= ((1 - (\beta_3^T X)^2)^{1/2} \cos(\pi\beta_1^T X), (1 - (\beta_3^T X)^2)^{1/2} \sin(\pi\beta_1^T X), \beta_3^T X) \\ \varepsilon &= \delta_1 v_1 + \delta_2 v_2, \end{aligned}$$

where $\delta_{1,2} \sim N(0, 0.2^2)$ and v_1, v_2 are orthogonal basis of the tangent space $T_{m(X)}\mathbb{S}^2$. The underlying subspace is $\mathcal{S} = [\beta_1, \beta_3]$.

- (3) Y is generated by

$$Y = (\sin(\beta_1^T X + \delta_1) \sin(\beta_2^T X + \delta_2), \sin(\beta_1^T X + \delta_1) \cos(\beta_2^T X + \delta_2), \cos(\beta_1^T X + \delta_1))$$

with $\delta_{1,2} \sim \mathcal{N}(0, 0.2^2)$. The underlying subspace is $\mathcal{S} = [\beta_1, \beta_2]$.

By applying the Gaussian kernel function, we estimate Fréchet central subspace using Fd-SDR, FOPG, and GWIRE. The simulation is repeated 100 times, and the means and standard deviations of the estimation errors for the three estimators are summarized in Table 3.

The simulation results in Table 3 demonstrate that Fd-SDR is competitive with FOPG and GWIRE in Model (1-a), (1-b) and (2-a), while achieving smaller errors in other three models for both cases of $n = 200, p = 10$ and $n = 400, p = 20$. We conclude that for the spherical data that generated in this scenario Fd-SDR can estimate the Fréchet subspace well and suit for the general settings of Fréchet SDR.

(n, p)	Model	Fd-SDR	FOPG	GWIRE
(200,10)	(1-a)	0.12 (0.06)	0.10 (0.05)	0.23 (0.10)
	(1-b)	0.15 (0.10)	0.13 (0.09)	0.49 (0.14)
	(2-a)	0.32 (0.18)	0.30 (0.18)	0.33 (0.23)
	(2-b)	0.39 (0.28)	0.40 (0.29)	0.69 (0.26)
	(3-a)	0.23 (0.14)	0.29 (0.30)	0.79 (0.44)
	(3-b)	0.26 (0.10)	0.31 (0.26)	0.85 (0.24)
(400,20)	(1-a)	0.12 (0.06)	0.11 (0.05)	0.21 (0.10)
	(1-b)	0.16 (0.17)	0.15 (0.17)	0.49 (0.15)
	(2-a)	0.37 (0.28)	0.39 (0.31)	0.30 (0.31)
	(2-b)	0.41 (0.23)	0.46 (0.29)	0.66 (0.23)
	(3-a)	0.25 (0.15)	0.39 (0.37)	0.65 (0.45)
	(3-b)	0.28 (0.09)	0.45 (0.36)	0.90 (0.28)

Table 3: Errors of Fd-SDR, FOPG and GWIRE in mean and standard deviation (in parentheses) for Scenario III. Here Fd-SDR uses the $\hat{\mathcal{S}}^{\text{GWIRE}}$ as the initialization.

4.4 Running Time Comparison

As outlined in Section 2.3, we previously discussed the computational complexity of the proposed method, Fd-SDR, and demonstrated its computational advantage over existing Fréchet SDR methods such as FOPG and GWIRE. In this section, we provide a numerical verification of this advantage by comparing the running times of Fd-SDR, FOPG, and GWIRE using the settings in Sections 4.1-4.3. All simulations were performed in Python on a machine equipped with an AMD Ryzen 5 5600X 6-core processor.

Table 4 presents the running times for each scenario with $(n, p) = (400, 20)$. The results demonstrate that Fd-SDR is considerably faster than both FOPG and GWIRE across all settings, achieving speeds 10 to 20 times faster than FOPG and 50 to 100 times faster than GWIRE. These findings confirm that Fd-SDR is significantly more efficient than FOPG and GWIRE in all cases. It is worth noting that Fd-SDR computes the kernel matrix only once outside the iterative process, while the other two methods require the kernel matrix to be recalculated in each iteration.

	Model	Fd-SDR	FOPG	GWIRE
Scenario I	(1-a)	0.07 (0.01)	2.52 (0.17)	3.37 (2.50)
	(1-b)	0.06 (0.01)	2.62 (0.12)	12.24 (0.54)
	(2-a)	0.03 (0.01)	0.19 (0.02)	2.17 (1.31)
	(2-b)	0.17 (0.02)	2.66 (0.10)	12.46 (0.36)
	(3-c), $\alpha = 0.2$	0.38 (0.06)	2.63 (0.11)	12.47 (0.46)
	(3-c), $\alpha = 0.4$	0.95 (0.27)	2.66 (0.09)	12.61 (0.59)
	(4-c), $\alpha = 0.2$	0.25 (0.03)	2.65 (0.12)	12.63 (0.39)
	(4-c), $\alpha = 0.4$	0.38 (0.08)	2.61 (0.10)	12.62 (1.70)
Scenario II	(1-a)	0.16 (0.12)	2.76 (0.10)	5.42 (2.37)
	(1-b)	0.09 (0.02)	2.84 (0.14)	15.82 (0.88)
	(2-a)	0.29 (0.38)	2.88 (0.13)	6.17 (3.14)
	(2-b)	0.14 (0.04)	2.79 (0.09)	15.46 (0.47)
Scenario III	(1-a)	0.06 (0.02)	2.56 (0.20)	3.38 (2.79)
	(1-b)	0.07 (0.08)	2.52 (0.06)	11.79 (0.38)
	(2-a)	0.54 (0.67)	2.53 (0.09)	3.02 (2.39)
	(2-b)	0.56 (0.54)	2.61 (0.07)	12.03 (0.33)
	(3-a)	0.46 (0.46)	2.63 (0.13)	3.48 (2.75)
	(3-b)	0.36 (0.22)	2.71 (0.22)	12.41 (0.59)

Table 4: Running time comparison (mean and standard deviation (in parenthesis), seconds) across Scenarios I, II, and III with $(n, p) = (400, 20)$.

5 Real Data Applications

In this section, we test the proposed Fd-SDR method on four real-world datasets: global human mortality data, Washington D.C. bike rental count data, gene expression data from eleven types of carcinoma, and breast cancer survival data.

5.1 Global Human Mortality Data

In this section, we demonstrate our method by applying it to the global human mortality dataset, which explores what influences human lifespans. This dataset captures age-at-death distributions, also referred to as mortality distributions, which are influenced by various factors such as economic conditions, health-care systems, and social and environmental determinants. Insights from this data are crucial for devel-

oping policies aimed at improving health outcomes and extending life expectancy.

The dataset was sourced from the UN World Population Prospects 2019 Database (available at <https://population.un.org/wpp/Download>). Nine predictors were used in the experiments:

- Population Density: population per square kilometer.
- Sex Ratio: number of males per 100 females in the population.
- Mean Childbearing Age: average age of mothers at childbirth.
- Gross Domestic Product (GDP) per Capita
- Gross Value Added (GVA) by Agriculture: percentage of GVA contributed by agriculture, hunting, forestry, and fishing.
- Consumer Price Index (CPI): relative to the base year 2010.
- Unemployment Rate.
- Expenditure on Health: as a percentage of GDP.
- Arable Land: percentage of total land area. These predictors were gathered from United Nations databases.

This dataset offers a comprehensive view of demographic metrics, particularly mortality patterns across countries and regions. By examining age-specific mortality distributions, this data helps identify trends and disparities, offering valuable insights for global health policy.

Following the settings described in (Zhang et al., 2023), we analyzed life tables for each country and age group. The tables record the number of deaths $d(x, n)$ aggregated every five years. These data were treated as histograms, with bin widths of five years. For 162 countries in 2015, we smoothed these histograms using the ‘frechet’ R package to obtain smoothed probability density functions. We then computed Wasserstein distances between the smoothed distributions. Additionally, we used a Gaussian kernel $\kappa(y, y') = \exp(-\gamma d_W^2(y, y'))$, with details provided in Section 2.2. We estimate the Fréchet central subspace by Fd-SDR, FOPG and GWIRE with $d = 3$ and subsequently fit the projected data, $\hat{\beta}^T \mathbf{X}$, using linear, polynomial and Fréchet regression (Petersen and Müller, 2019). The adjusted R-squared values are provided in Table 5. The R-squared of Fd-SDR and GWIRE methods are close and

both of them better than FOPG method (Table 5). Figure 2 (a) shows the mortality rate over ages versus the 1st sufficient predictor. (b) and (c) show that the mean and standard deviation of age at death of each country versus the 1st and 2nd sufficient predictors.

Metric	Fd-SDR	FOPG	GWIRE
Adjusted R-squared	0.542	0.415	0.561
Fréchet R-squared	0.544	0.386	0.562
Poly R-squared	0.929	0.932	0.933

Table 5: Performance metrics for the global mortality data

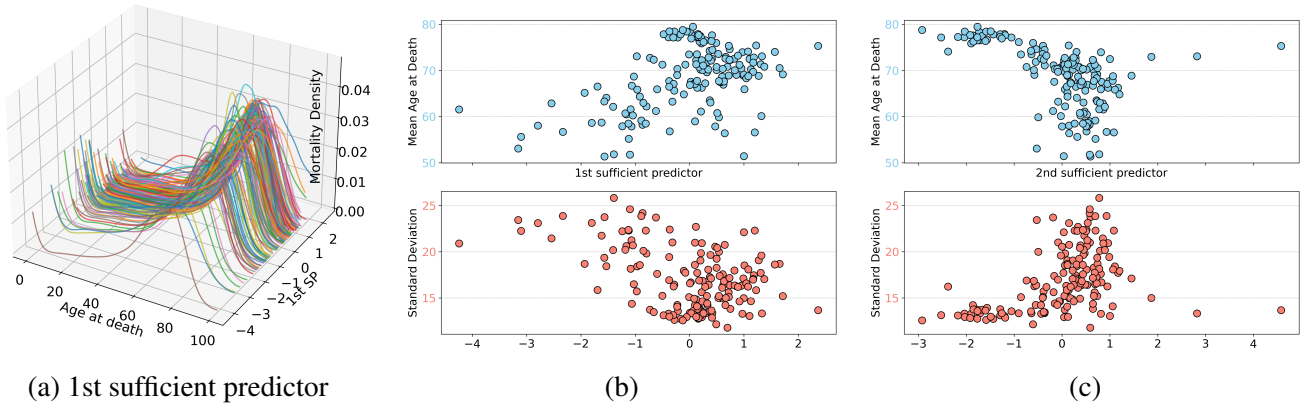


Figure 2: (a) Global mortality rate by age (in years) plotted against the first sufficient predictor; (b) Mean mortality distribution versus the first two sufficient predictors; (c) Standard deviation of mortality distribution versus the first two sufficient predictors.

5.2 Bike Rental Data

In this section, we apply our proposed method to bike rental data (Fanaee-T and Gama, 2014). The bike rental data from the UCI Machine Learning Repository is a widely-used dataset that captures bike-sharing usage patterns in Washington, D.C. The data spans two years (2011–2012) and includes hourly and daily counts of bike rentals, along with information on weather conditions, seasonal effects, holidays, and time-based features such as hour and weekday. This dataset is ideal for exploring temporal patterns in bike rentals, assessing the impact of external factors like weather and holidays on usage, and developing predictive models for demand forecasting. We follow the settings from (Weng et al., 2023) and choose 6 predictors similar to (Weng et al., 2023): 1) Holiday: Indicator of a public holiday celebrated in

Washington D.C. 2) Workingday: Indicator of neither the weekend nor a holiday 3) Temp: Daily mean temperature 4) Atemp: Feeling temperature 5) BW: Indicator of bad weather 6) RBW: Indicator of really bad weather.

In this dataset, we set $d = 2$ to estimate the Fréchet central subspace with the Gaussian kernel $\kappa(y, y') = \exp(-\gamma d_W^2(y, y'))$. We fit the estimated projected data, $\hat{\beta}^T \mathbf{X}$, using linear, polynomial and Fréchet regression (Petersen and Müller, 2019). The corresponding values of R squares are presented in Table 6 and the coefficients of the estimated subspace are given in Table 7. Among the three methods, Fd-SDR has the highest R-squared values in all regression models. In addition, we display the bike rental count data over time (by hour) against the first and second sufficient predictors in Figures 3 and 4, respectively. Figure 3 (a) illustrates all curves for both working and nonworking days, while Figures 3(b) and (c) separately depict the curves for working and non-working days, respectively. Based on the curve patterns shown in Figure 3, it is evident that bike rentals are common in the morning before 8 AM and in the afternoon around 6 PM. On non-working days, people predominantly rent bikes before 12 PM. We infer that on working days, most bike rentals are for commuting, whereas on non-working days, people complete their outdoor activities in the morning.

Furthermore, Table 7 indicates that Fd-SDR identifies two types of factors influencing bike rentals. The first type consists of individuals who commute using rental bikes ($\hat{\beta}_1$ shows a high loading on the predictor “Working”) and who consider the perceived temperature (“Atemp” coefficient is larger than other predictors in magnitude). The second type comprises those who rent bikes mainly for entertainment, where temperature and weather are the primary factors (see coefficients for $\hat{\beta}_2$). The results obtained by Fd-SDR align with common observations.

Metric	Fd-SDR	FOPG	GWIRE
Adjusted R-squared	0.519	0.361	0.504
Fréchet R-squared	0.367	0.344	0.365
Polynomial R-squared	0.783	0.704	0.769

Table 6: Performance metrics for the bike rental data

Feature	$\hat{\beta}_1$	$\hat{\beta}_2$
Holiday	-0.01	-0.07
Working	-0.99	-0.15
Temp	0.05	-0.79
Atemp	-0.13	1.7
BW	-0.02	0.16
RBW	0.03	-0.2

Table 7: Coefficients of the two directions $\hat{\beta}_1$ and $\hat{\beta}_2$ for the bike rental data, which are obtained by Fd-SDR.

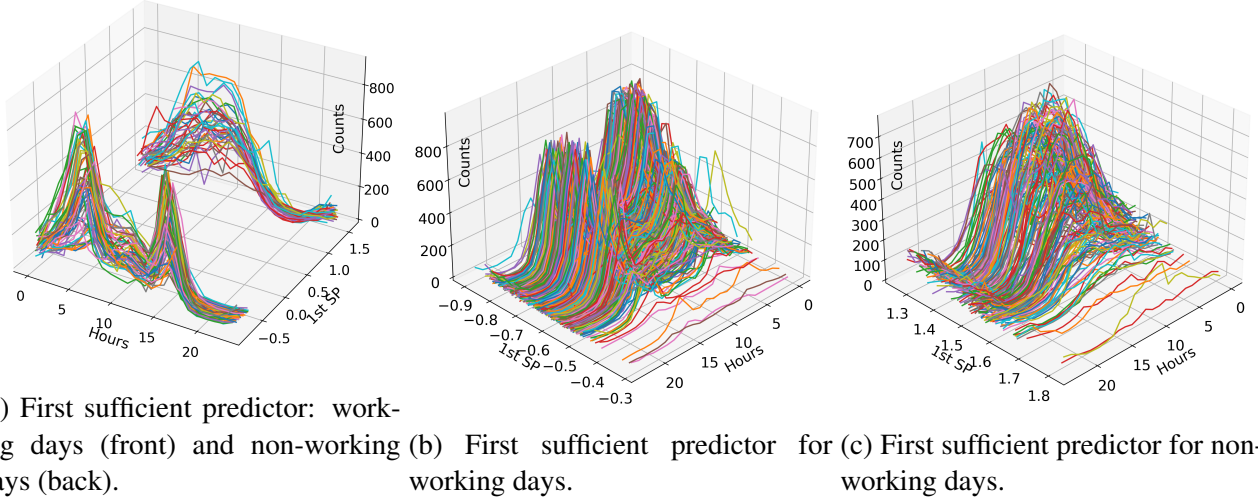


Figure 3: The bike rental count data over time (by hour) projected onto the first sufficient predictor in (a) and onto the first sufficient predictors in (b) and (c).

5.3 Ultrahigh-Dimensional Analysis: Carcinomas Data

Carcinoma, a type of cancer originating in epithelial cells that form the skin or line internal organs, requires precise classification based on primary anatomical sites (e.g., prostate, liver) to guide optimal treatment strategies (Su et al., 2001). This study examines the carcinomas dataset (U95a GeneChip) from (Su et al., 2001), comprising $n = 174$ samples spanning 11 carcinoma types: prostate, bladder/ureter, breast, colorectal, gastroesophageal, kidney, liver, ovary, pancreas, lung adenocarcinoma, and lung squamous cell carcinoma. For clarity, we denote these types as classes 0 through 10 in our experiments. The respective sample sizes are 26, 8, 26, 23, 12, 11, 7, 27, 6, 14, and 14. Collectively, these carcinoma types account for approximately 70% of cancer-related deaths in the United States (Su et al., 2001).

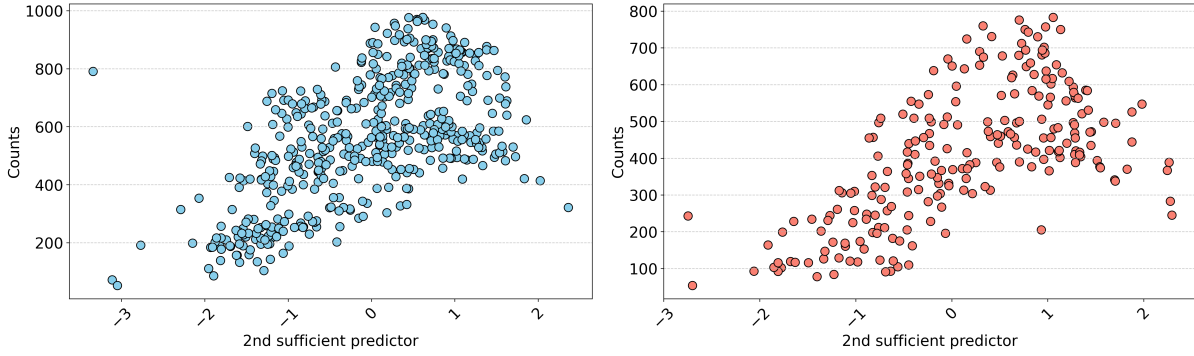


Figure 4: Plots of the maximum counts of bike rental distributions versus the second sufficient predictor on working days (left) and non-working days (right).

Each sample provides gene expression levels for $p = 9183$ predictors, which have been preprocessed as described by (Su et al., 2001). The primary goal of this analysis is to classify carcinoma types based on gene expression profiles and identify genes significantly associated with each carcinoma category.

We applied the proposed Fd-SDR method to this dataset, treating carcinoma types as the response variable. To reduce dimensionality, we employed the Ball Correlation Sure Independence Screening (BCor-SIS) method (Pan et al., 2019), which reduced the number of predictors to 173. Fd-SDR, FOPG, and GWIRE with a Gaussian kernel are then used to estimate the Fréchet central subspace with dimension $d = 2$. Logistic regression was then performed using $\hat{\beta}^T \mathbf{X}$ as the predictors and \mathbf{Y} as the responses. Model performance was evaluated using the area under the curve (AUC) metric. The mean and standard deviation of the AUC scores, obtained through 5-fold cross-validation, are presented in Table 8. As shown, Fd-SDR achieved the highest AUC, outperforming both FOPG and GWIRE.

We also visualize the projected data $(\hat{\beta}^{\text{Fd-SDR}})^T \mathbf{X}$ in Figure 5. The plot reveals clear separation among most carcinoma types, with some overlap observed between colorectal, kidney, and ovarian carcinomas (classes 4, 6, and 8). This highlights the effectiveness of our proposed method. The observed overlaps are likely due to shared genomic mutations and similar metastatic patterns, as noted in (Kan et al., 2010; Kir et al., 2010).

Method	Fd-SDR	FOPG	GWIRE
AUC	0.796 (0.180)	0.515 (0.155)	0.714 (0.213)

Table 8: AUC Mean with standard deviation (in parentheses) for logistic regression.

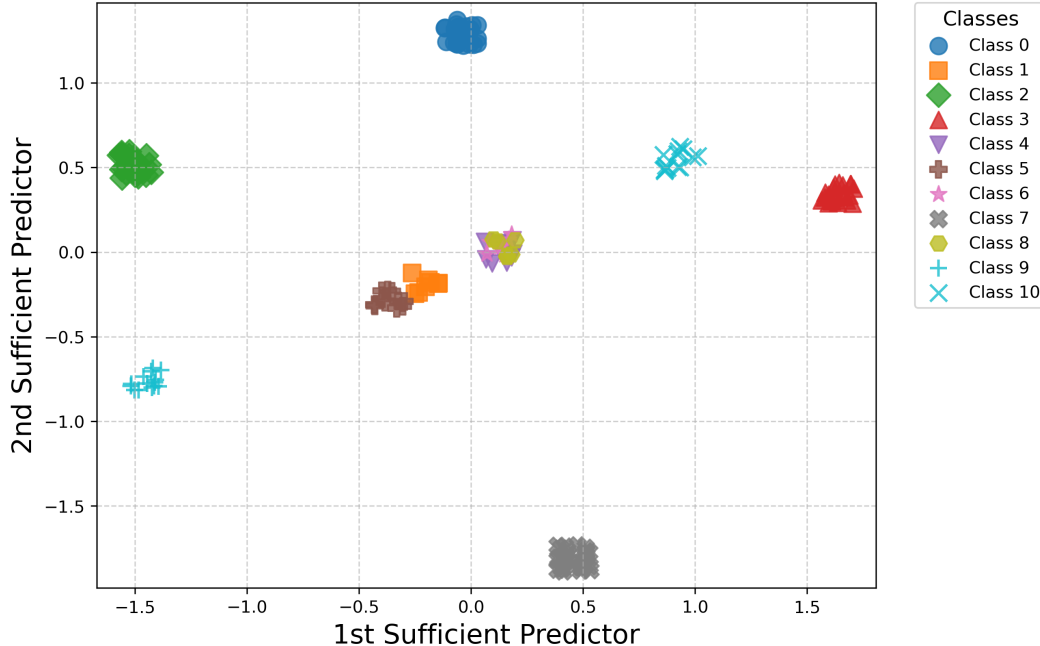


Figure 5: Scatter plot of the first two sufficient predictors for the carcinoma data, with labels ranging from 0 to 10.

5.4 Ultrahigh-Dimensional Analysis: TCGA Breast Cancer Survival Data

The last experiment to test the proposed method is the Breast Cancer dataset from The Cancer Genome Atlas (TCGA), utilizing three sources of data: gene expression RNAseq (IlluminaHiSeq percentile), curated survival endpoints, and clinical data obtained from the Xena platform (Goldman et al., 2020). The goal of this experiment to investigate the relationship between overall survival time and gene expressions.

The gene expression dataset consists of 1,218 samples and 20,531 genes. The curated survival data includes four types of survival endpoints for each TCGA cancer type: Overall Survival (OS), Progression-Free Interval (PFI), Disease-Free Interval (DFI), and Disease-Specific Survival (DSS). Additionally, the clinical dataset provides information on each patient’s age at the time of initial pathological diagnosis.

We divided all samples into 34 age-based groups and calculated the survival time distributions for each group. The average gene expression within each group was used as predictors. Since the dimensionality is much larger than the number of samples, we applied the BCor-SIS method (Pan et al., 2019) to reduce the dimensionality. We then applied the Fd-SDR, FOPG, and GWIRE methods to estimate the Fréchet central subspace with a dimension of $d = 3$. The estimated projected data, $\hat{\beta}^T \mathbf{X}$, was fitted using

linear, polynomial and Fréchet regression. The R-squared values are presented in Table 9, demonstrating that Fd-SDR has the highest values and outperforms the other two methods in both linear and Fréchet regression models. Since all three estimators achieve exceptional performance with R-squared values of 0.99 for polynomial regression, these results are omitted from Table 9.

Metric	Fd-SDR	FOPG	GWIRE
Adjusted R-squared	0.661	0.645	0.648
Fréchet R-squared	0.702	0.688	0.691

Table 9: R-squared metrics for the breast cancer survival data.

6 Discussion

In classical regression, SDR is a powerful tool for exploratory data analysis, regression diagnostics, and mitigating the curse of dimensionality. By addressing challenges such as collinearity among predictors, heteroscedasticity in the response, and identifying the most critical linear combinations of predictors, SDR facilitates more efficient and interpretable data analysis. By examining scatter plots of the response against the first two sufficient predictors derived via SDR, one can visualize and explore the general shape of the regression surface without resorting to complex models. These visualizations are especially valuable for uncovering and interpreting relationships in high-dimensional settings.

In our proposed method, the projection of mortality density onto the first sufficient predictor within the CMS effectively captures key patterns across various applications, including mortality distributions between countries, bike rental count distributions, carcinoma clusters in two-dimensional projection plots, and breast cancer survival data. For example, in the case of mortality data, the lower end of the sufficient predictor reveals a shift toward higher longevity, while the upper end highlights lower longevity with a marked increase near age 0, reflecting infant mortality. These results highlight the capability of CMS to condense complex, multivariate relationships into an interpretable low-dimensional representation.

A key innovation of our approach is the integration of kernel distance covariance into the SDR framework, which enhances the detection of complex and non-linear functional relationships. Traditional SDR methods often emphasize linear dependencies, which can limit their ability to uncover more intricate associations. By incorporating kernel distance covariance, our method expands the scope of SDR, allowing

it to capture a broader range of associations and achieve more flexible and precise dimension reduction. This advancement broadens the applicability of SDR to accommodate response variables valued in metric spaces, with the CMS framework providing a solid foundation for identifying sufficient predictors. Furthermore, our methodology applies to any separable and complete metric space of negative type, greatly expanding the potential applications of SDR and offering a robust framework for Fréchet regression in diverse data settings.

In conclusion, the integration of kernel distance covariance within the CMS framework greatly enhances the applicability and versatility of SDR for analyzing metric-space-valued data. This advancement facilitates the discovery of complex relationships in high-dimensional settings, representing a significant step forward in the theory and practice of sufficient dimension reduction.

Funding

We gratefully acknowledge the support of the *National Science Foundation* through grants (DMS-1924792, DMS-2318925 and CNS-1818500).

References

- P-A Absil and Jérôme Malick. Projection-like retractions on matrix manifolds. *SIAM Journal on Optimization*, 22(1):135–158, 2012.
- P-A Absil, Robert Mahony, and Rodolphe Sepulchre. *Optimization algorithms on matrix manifolds*. Princeton University Press, 2008.
- R Dennis Cook and Sanford Weisberg. Discussion of sliced inverse regression for dimension reduction. *Journal of the American Statistical Association*, 86(414):328–332, 1991.
- R.Dennis Cook and Bing Li. Dimension reduction for conditional mean in regression. *The Annals of Statistics*, 30(2):455 – 474, 2002. doi: 10.1214/aos/1021379861. URL <https://doi.org/10.1214/aos/1021379861>.
- Hadi Fanaee-T and Joao Gama. Event labeling combining ensemble detectors and background knowledge. *Progress in Artificial Intelligence*, 2:113–127, 2014.

- Maurice Fréchet. Les éléments aléatoires de nature quelconque dans un espace distancié. *Annales de l'institut Henri Poincaré*, 10(4):215–310, 1948.
- Mary J Goldman, Brian Craft, Mim Hastie, Kristupas Repečka, Fran McDade, Akhil Kamath, Ayan Banerjee, Yunhai Luo, Dave Rogers, Angela N Brooks, et al. Visualizing and interpreting cancer genomics data via the xena platform. *Nature biotechnology*, 38(6):675–678, 2020.
- Peter Hall and Ker-Chau Li. On almost linearity of low dimensional projections from high dimensional data. *The annals of Statistics*, pages 867–889, 1993.
- Hsin-Hsiung Huang, Feng Yu, and Teng Zhang. Robust sufficient dimension reduction via α -distance covariance. *Journal of Nonparametric Statistics*, pages 1–16, 2024.
- Zhengyan Kan, Bijay S Jaiswal, Jeremy Stinson, Vasantharajan Janakiraman, Deepali Bhatt, Howard M Stern, Peng Yue, Peter M Haverty, Richard Bourgon, Jianbiao Zheng, et al. Diverse somatic mutation patterns and pathway alterations in human cancers. *Nature*, 466(7308):869–873, 2010.
- Gozde Kir, Ayse Gurbuz, Ates Karateke, and Mustafa Kir. Clinicopathologic and immunohistochemical profile of ovarian metastases from colorectal carcinoma. *World journal of gastrointestinal surgery*, 2(4):109, 2010.
- Ker-Chau Li. Sliced inverse regression for dimension reduction. *Journal of the American Statistical Association*, 86(414):316–327, 1991. doi: 10.1080/01621459.1991.10475035. URL <https://www.tandfonline.com/doi/abs/10.1080/01621459.1991.10475035>.
- Lexin Li and Xiangrong Yin. Sliced inverse regression with regularizations. *Biometrics*, 64(1):124–131, 2008.
- Charles A. Micchelli, Yuesheng Xu, and Haizhang Zhang. Universal kernels. *Journal of Machine Learning Research*, 7(95):2651–2667, 2006. URL <http://jmlr.org/papers/v7/micchelli06a.html>.
- Wenliang Pan, Xueqin Wang, Weinan Xiao, and Hongtu Zhu. A generic sure independence screening procedure. *Journal of the American Statistical Association*, 114(526):928–937, 2019.

- Alexander Petersen and Hans-Georg Müller. Fréchet regression for random objects with Euclidean predictors. *The Annals of Statistics*, 47(2):691–719, 2019.
- Armin Schwartzman. *Random ellipsoids and false discovery rates: Statistics for diffusion tensor imaging data*. Stanford University, 2006.
- Dino Sejdinovic, Bharath Sriperumbudur, Arthur Gretton, and Kenji Fukumizu. Equivalence of distance-based and rkhs-based statistics in hypothesis testing. *The annals of statistics*, pages 2263–2291, 2013.
- Wenhui Sheng and Xiangrong Yin. Direction estimation in single-index models via distance covariance. *Journal of Multivariate Analysis*, 122:148–161, 2013.
- Wenhui Sheng and Xiangrong Yin. Sufficient dimension reduction via distance covariance. *Journal of Computational and Graphical Statistics*, 25(1):91–104, 2016.
- Bharath K. Sriperumbudur, Kenji Fukumizu, and Gert R.G. Lanckriet. Universality, characteristic kernels and rkhs embedding of measures. *Journal of Machine Learning Research*, 12(70):2389–2410, 2011. URL <http://jmlr.org/papers/v12/sriperumbudur11a.html>.
- GW Stewart. Matrix perturbation theory. *Computer Science and Scientific Computing/Academic Press, Inc*, 1990.
- Andrew I Su, John B Welsh, Lisa M Sapinoso, Suzanne G Kern, Petre Dimitrov, Hilmar Lapp, Peter G Schultz, Steven M Powell, Christopher A Moskaluk, Henry F Frierson Jr, et al. Molecular classification of human carcinomas by use of gene expression signatures. *Cancer Research*, 61(20):7388–7393, 2001.
- Gábor J. Székely, Maria L. Rizzo, and Nail K. Bakirov. Measuring and testing dependence by correlation of distances. *The Annals of Statistics*, 35(6):2769 – 2794, 2007. doi: 10.1214/009053607000000505. URL <https://doi.org/10.1214/009053607000000505>.
- Kean Ming Tan, Zhaoran Wang, Tong Zhang, Han Liu, and R Dennis Cook. A convex formulation for high-dimensional sparse sliced inverse regression. *Biometrika*, 105(4):769–782, 2018.
- Jiaying Weng, Kai Tan, Cheng Wang, and Zhou Yu. Sparse Fréchet sufficient dimension reduction with graphical structure among predictors. *arXiv preprint arXiv:2310.19114*, 2023.

- Yingcun Xia, Howell Tong, Wai Keung Li, and Li-Xing Zhu. An adaptive estimation of dimension reduction space. *Journal of the Royal Statistical Society Series B: Statistical Methodology*, 64(3): 363–410, 2002.
- Xing Yang and Jianjun Xu. Functional sufficient dimension reduction through distance covariance. *Journal of Statistical Computation and Simulation*, pages 1–22, 2024.
- Xiangrong Yin and R Dennis Cook. Direction estimation in single-index regressions. *Biometrika*, 92(2): 371–384, 2005.
- Xiangrong Yin and Bing Li. Sufficient dimension reduction based on an ensemble of minimum average variance estimators. *The Annals of Statistics*, 39(6):3392 – 3416, 2011. doi: 10.1214/11-AOS950. URL <https://doi.org/10.1214/11-AOS950>.
- Chao Ying and Zhou Yu. Fréchet sufficient dimension reduction for random objects. *Biometrika*, 109 (4):975–992, 2022.
- Jia Zhang and Xin Chen. Robust sufficient dimension reduction via ball covariance. *Computational Statistics & Data Analysis*, 140:144–154, 2019.
- Nan Zhang and Xiangrong Yin. Direction estimation in single-index regressions via hilbert-schmidt independence criterion. *Statistica Sinica*, pages 743–758, 2015.
- Qi Zhang, Lingzhou Xue, and Bing Li. Dimension reduction for Fréchet regression. *Journal of the American Statistical Association*, pages 1–15, 2023.